

9-2009

# Evidence for reversible control of magnetization in a ferromagnetic material by means of spin-orbit magnetic field

Alexandr Chernyshov  
*Purdue University - Main Campus*

Mason Overby  
*Purdue University, maoverby@purdue.edu*

Xinyu Liu  
*University of Notre Dame*

Jacek Furdyna  
*University of Notre Dame*

Yuli Lyanda-Geller  
*Purdue University, yuli@purdue.edu*

*See next page for additional authors*

Follow this and additional works at: <http://docs.lib.purdue.edu/nanopub>

 Part of the [Nanoscience and Nanotechnology Commons](#)

Chernyshov, Alexandr; Overby, Mason; Liu, Xinyu; Furdyna, Jacek; Lyanda-Geller, Yuli; and Rokhinson, Leonid P., "Evidence for reversible control of magnetization in a ferromagnetic material by means of spin-orbit magnetic field" (2009). *Birck and NCN Publications*. Paper 571.  
<http://docs.lib.purdue.edu/nanopub/571>

This document has been made available through Purdue e-Pubs, a service of the Purdue University Libraries. Please contact [epubs@purdue.edu](mailto:epubs@purdue.edu) for additional information.

---

**Authors**

Alexandr Chernyshov, Mason Overby, Xinyu Liu, Jacek Furdyna, Yuli Lyanda-Geller, and Leonid P. Rokhinson

# Evidence for reversible control of magnetization in a ferromagnetic material by means of spin-orbit magnetic field

Alexandr Chernyshov<sup>1\*</sup>, Mason Overby<sup>1\*</sup>, Xinyu Liu<sup>2</sup>, Jacek K. Furdyna<sup>2</sup>, Yuli Lyanda-Geller<sup>1</sup> and Leonid P. Rokhinson<sup>1†</sup>

The current state of information technology accentuates the dichotomy between processing and storage of information, with logical operations carried out by charge-based devices and non-volatile memory based on magnetic materials. The main obstacle for a wider use of magnetic materials for information processing is the lack of efficient control of magnetization. Reorientation of magnetic domains is conventionally carried out by non-local external magnetic fields or by externally polarized currents<sup>1–3</sup>. The efficiency of the latter approach is enhanced in materials where ferromagnetism is carrier-mediated<sup>4</sup>, because in such materials the control of carrier polarization provides an alternative means for manipulating the orientation of magnetic domains. In some crystalline conductors, the charge current couples to the spins by means of intrinsic spin-orbit interactions, thus generating non-equilibrium electron spin polarization<sup>5–11</sup> tunable by local electric fields. Here, we show that magnetization can be reversibly manipulated by the spin-orbit-induced polarization of carrier spins generated by the injection of unpolarized currents. Specifically, we demonstrate domain rotation and hysteretic switching of magnetization between two orthogonal easy axes in a model ferromagnetic semiconductor.

In crystalline materials with inversion asymmetry, intrinsic spin-orbit interactions couple the electron spin with its momentum  $\hbar\mathbf{k}$ . The coupling is given by the Hamiltonian  $\mathcal{H}_{\text{so}} = (\hbar/2)\hat{\sigma} \cdot \mathbf{\Omega}(\mathbf{k})$ , where  $\hbar$  is the reduced Planck constant and  $\hat{\sigma}$  is the electron spin operator (for holes  $\hat{\sigma}$  should be replaced by the total angular momentum  $\mathbf{J}$ ). Electron states with different spin projection signs on  $\mathbf{\Omega}(\mathbf{k})$  are split in energy, analogous to the Zeeman splitting in an external magnetic field. In zinc-blende crystals such as GaAs there is a cubic Dresselhaus term<sup>12</sup>  $\mathbf{\Omega}_D \propto k^3$ , whereas strain introduces a term  $\mathbf{\Omega}_\varepsilon = C\Delta\varepsilon(k_x, -k_y, 0)$  that is linear in  $k$ , where  $\Delta\varepsilon$  is the difference between strain in the  $z$  and  $x, y$  directions<sup>13</sup>. In wurtzite crystals or in multilayered materials with structural inversion asymmetry, there also exists the Rashba term<sup>14</sup>  $\mathbf{\Omega}_R$ , which has a different symmetry with respect to the direction of  $k$ ,  $\mathbf{\Omega}_R = \alpha_R(-k_y, k_x, 0)$ , where  $z$  is along the axis of reduced symmetry. In the presence of an electric field, the electrons acquire an average momentum  $\hbar\Delta\mathbf{k}(\mathbf{E})$ , which leads to the generation of an electric current  $\mathbf{j} = \hat{\rho}^{-1}\mathbf{E}$  in the conductor, where  $\hat{\rho}$  is the resistivity tensor. This current defines the preferential axis for spin precession  $\langle\mathbf{\Omega}(\mathbf{j})\rangle$ . As a result, a non-equilibrium current-induced spin polarization  $\langle\mathbf{J}^E\rangle \parallel \langle\mathbf{\Omega}(\mathbf{j})\rangle$  is generated, the magnitude of which  $\langle\mathbf{J}^E\rangle$  depends on the strength of various mechanisms of momentum scattering

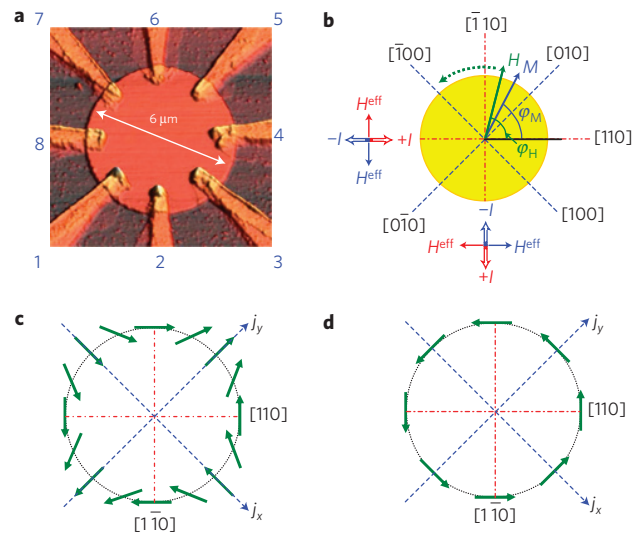


**Figure 1 | Layout of the device and symmetry of the spin-orbit fields.**

**a**, Atomic force micrograph of sample A with eight non-magnetic metal contacts. **b**, Diagram of device orientation with respect to crystallographic axes, with easy and hard magnetization axes marked with blue dashed and red dot-dash lines, respectively. Measured directions of  $\mathbf{H}^{\text{eff}}$  field are shown for different current directions. **c,d**, Orientation of effective magnetic field with respect to current direction for strain-induced (**c**) and Rashba (**d**) spin-orbit interactions. The current-induced Oersted field under the contacts has the same symmetry as the Rashba field.

and spin relaxation<sup>5,15</sup>. This spin polarization has been measured in non-magnetic semiconductors using optical<sup>7–9,11,16</sup> and electron spin resonance<sup>17</sup> techniques. It is convenient to parameterize  $\langle\mathbf{J}^E\rangle$  in terms of an effective magnetic field  $\mathbf{H}^{\text{so}}$ . Different contributions to  $\mathbf{H}^{\text{so}}$  have different current dependencies ( $\propto j$  or  $j^3$ ), as well as different symmetries with respect to the direction of  $\mathbf{j}$ , as schematically shown in Fig. 1c,d, enabling one to distinguish between spin polarizations in different fields.

To investigate interactions between the spin-orbit-generated magnetic field and magnetic domains, we have chosen (Ga,Mn)As, a p-type ferromagnetic semiconductor<sup>18,19</sup> with zinc-blende crystalline structure similar to GaAs. Ferromagnetic interactions in this material are carrier-mediated<sup>20,21</sup>. The total angular momentum of the holes  $\mathbf{J}$  couples to the magnetic moment  $\mathbf{F}$  of Mn ions by means

<sup>1</sup>Department of Physics and Birk Nanotechnology Center, Purdue University, West Lafayette, Indiana 47907, USA, <sup>2</sup>Department of Physics, University of Notre Dame, Notre Dame, Indiana 46556, USA. \*These authors contributed equally to this work. †e-mail: leonid@purdue.edu.

of antiferromagnetic exchange  $\mathcal{H}_{\text{ex}} = -\mathbf{A}\mathbf{F}\cdot\mathbf{J}$ . This interaction leads to the ferromagnetic alignment of magnetic moments of Mn ions and equilibrium polarization of hole spins. If further, non-equilibrium spin polarization of the holes ( $\mathbf{J}^{\text{E}}$ ) is induced, the interaction of the hole spins with magnetic moments of Mn ions enables one to control ferromagnetism by manipulating  $\mathbf{J}$ . Magnetic properties of (Ga,Mn)As are thus tightly related to the electronic properties of GaAs. For example, strain-induced spin anisotropy of the hole energy dispersion is largely responsible for the magnetic anisotropy in this material. (Ga,Mn)As, epitaxially grown on the (001) surface of GaAs, is compressively strained, which results in magnetization  $\mathbf{M}$  lying in the plane of the layer perpendicular to the growth direction, with two easy axes along the [100] and [010] crystallographic directions<sup>22,23</sup>. Recently, control of magnetization by means of strain modulation has been demonstrated<sup>24</sup>. In this letter, we use spin-orbit-generated polarization ( $\mathbf{J}^{\text{E}}$ ) to manipulate ferromagnetism.

We report measurements on two samples fabricated from (Ga,Mn)As wafers with different Mn concentrations. The devices were patterned into circular islands with eight non-magnetic ohmic contacts, as shown in Fig. 1a and discussed in the Methods section. In the presence of a strong external magnetic field  $\mathbf{H}$ , the magnetization of the ferromagnetic island is aligned with the field. For weak fields, however, the direction of magnetization is primarily determined by magnetic anisotropy. As a small field ( $5 < H < 20$  mT) is rotated in the plane of the sample, the magnetization is re-aligned along the easy axis closest to the field direction. Such rotation of magnetization by an external field is demonstrated in Fig. 2. For the current  $\mathbf{I}||[1\bar{1}0]$ , the measured  $R_{xy}$  is positive for  $\mathbf{M}||[100]$  and negative for  $\mathbf{M}||[010]$ . Note that  $R_{xy}$ , and thus also the magnetization, switches direction when the direction of  $\mathbf{H}$  is close to the hard axes [110] and  $[1\bar{1}0]$ , confirming the cubic magnetic anisotropy of our samples. The switching angles  $\varphi_{\text{H}} = \angle\mathbf{H}\mathbf{I}$  where  $R_{xy}$  changes sign are denoted as  $\varphi_{\text{H}}^{(i)}$  on the plot.

In the presence of both external and spin-orbit fields, we expect to see a combined effect of  $\mathbf{H}^{\text{so}} + \mathbf{H}$  on the direction of magnetization. For small currents (a few microamperes)  $H^{\text{so}} \approx 0$ , and  $R_{xy}$  does not depend on the sign or the direction of the current. At large d.c. currents, the value of  $\varphi_{\text{H}}^{(i)}$  becomes current dependent and we define  $\Delta\varphi_{\text{H}}^{(i)}(I) = \varphi_{\text{H}}^{(i)}(I) - \varphi_{\text{H}}^{(i)}(-I)$ . Specifically, for  $\mathbf{I}||[1\bar{1}0]$ , the switching of magnetization  $[010] \rightarrow [100]$  occurs for  $I = +0.7$  mA at smaller  $\varphi_{\text{H}}^{(1)}$  than for  $I = -0.7$  mA,  $\Delta\varphi_{\text{H}}^{(1)} < 0$ . For the  $[0\bar{1}0] \rightarrow [100]$  magnetization switching, the  $I$  dependence of the switching angle is reversed,  $\Delta\varphi_{\text{H}}^{(3)} > 0$ . There is no measurable difference in switching angle for the  $[100] \rightarrow [010]$  and  $[100] \rightarrow [010]$  transitions ( $\Delta\varphi_{\text{H}}^{(2,4)} \approx 0$ ). When the current is rotated by  $90^\circ$  ( $\mathbf{I}||[110]$ ), we observe  $\Delta\varphi_{\text{H}}^{(2)} > 0$ ,  $\Delta\varphi_{\text{H}}^{(4)} < 0$  and  $\Delta\varphi_{\text{H}}^{(1,3)} \approx 0$ . Figure 2c shows that  $\Delta\varphi_{\text{H}}^{(i)}(I)$  decreases as current decreases and drops below experimental resolution of  $0.5^\circ$  at  $I < 50 \mu\text{A}$ . Similar data are obtained for sample B (see Supplementary Fig. S4).

The data can be qualitatively understood if we consider an extra current-induced effective magnetic field  $\mathbf{H}^{\text{eff}}$ , as shown schematically in Fig. 1b. When an external field  $\mathbf{H}$  aligns the magnetization along one of the hard axes, a small perpendicular field can initiate magnetization switching. For  $\mathbf{I}||[110]$ , the effective field  $\mathbf{H}^{\text{eff}}||[110]$  aids the  $[100] \rightarrow [010]$  magnetization switching, whereas it hinders the  $[100] \rightarrow [010]$  switching. For  $\varphi_{\text{H}} \approx 90^\circ$  and  $\varphi_{\text{H}}^{(3)} \approx 270^\circ$ , where  $[010] \rightarrow [100]$  and  $[0\bar{1}0] \rightarrow [100]$  magnetization transitions occur,  $\mathbf{H}^{\text{eff}}||\mathbf{H}$  does not affect the transition angle,  $\Delta\varphi_{\text{H}}^{(2,4)} = 0$ . For  $\mathbf{I}||[1\bar{1}0]$ , the direction of the field  $\mathbf{H}^{\text{eff}}||[110]$  is reversed relative to the direction of the current, compared with the  $\mathbf{I}||[110]$  case. The symmetry of the measured  $\mathbf{H}^{\text{eff}}$  with respect to  $\mathbf{I}$  coincides with the unique symmetry of the strain-related spin-orbit field (Fig. 1c).

The dependence of  $\Delta\varphi_{\text{H}}^{(i)}$  on various magnetic fields and current orientations is summarized in Fig. 3a,b. Assuming that the angle of

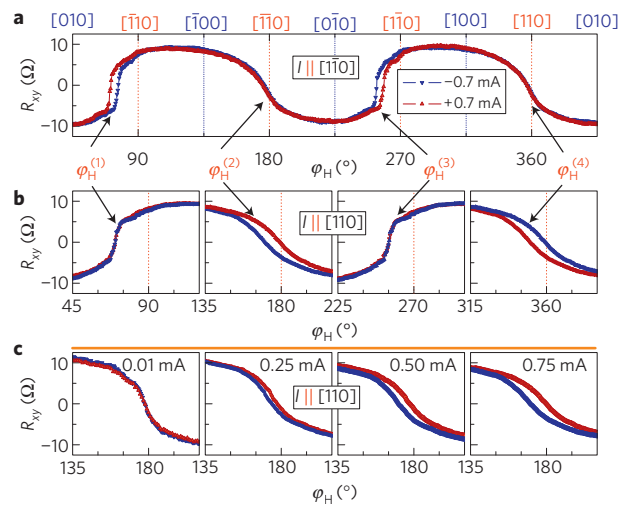


**Figure 2 | Dependence of transverse anisotropic magnetoresistance on current and field orientation.** **a, b**, Transverse anisotropic magnetoresistance  $R_{xy}$  as a function of external field direction  $\varphi_{\text{H}}$  for  $H = 10$  mT and current  $I = \pm 0.7$  mA in sample A. The angles  $\varphi_{\text{H}}^{(i)}$  mark magnetization switchings. **c**, Magnetization switching between  $[100]$  and  $[0\bar{1}0]$  easy axes for several values of the current.

magnetization switching depends only on the total field  $\mathbf{H}^{\text{eff}} + \mathbf{H}$ , we can extract the magnitude  $H^{\text{eff}}$  and angle  $\theta = \angle\mathbf{H}\mathbf{H}^{\text{eff}}$  from the measured  $\Delta\varphi_{\text{H}}^{(i)}$ , thus reconstructing the whole vector  $\mathbf{H}^{\text{eff}}$ . Following a geometrical construction shown in Fig. 3d and taking into account that  $\Delta\varphi_{\text{H}}^{(i)}$  is small, we find that

$$H^{\text{eff}} \approx H \sin(\Delta\varphi_{\text{H}}^{(i)}/2) / \sin(\theta - \varphi_{\text{H}}^{(i)})$$

and  $\theta$  can be found from the comparison of switching at two angles. We find that  $\theta \approx 90^\circ$ , or  $\mathbf{H}^{\text{eff}} \perp \mathbf{I}$  for  $\mathbf{I}||[110]$  and  $\mathbf{I}||[1\bar{1}0]$ . To further test our procedure, we carried out similar experiments with small current  $I = 10 \mu\text{A}$  but constant extra magnetic field  $\delta\mathbf{H} \perp \mathbf{I}$  having the role of  $\mathbf{H}^{\text{eff}}$ . The measured  $\delta H(\Delta\varphi_{\text{H}})$  coincides with the applied  $\delta H$  within the precision of our measurements. (See Supplementary Fig. S5.)

In Fig. 3c,  $H^{\text{eff}}$  is plotted as a function of the average current density  $\langle j \rangle$  for both samples. There is a small difference in the  $H^{\text{eff}}$  versus  $\langle j \rangle$  dependence for  $\mathbf{I}||[110]$  and  $\mathbf{I}||[1\bar{1}0]$ . The difference can be explained by considering the current-induced Oersted field  $H^{\text{Oe}} \propto I$  in the metal contacts. The Oersted field is localized under the pads, which constitutes only 7% (2.5%) of the total area for sample A (B). The Oersted field has the symmetry of the field shown in Fig. 1d, and is added to or subtracted from the spin-orbit field, depending on the current direction. Thus,  $H^{\text{eff}} = H^{\text{so}} + H^{\text{Oe}}$  for  $\mathbf{I}||[110]$  and  $H^{\text{eff}} = H^{\text{so}} - H^{\text{Oe}}$  for  $\mathbf{I}||[1\bar{1}0]$ . We estimate the fields to be as high as 0.6 mT under the contacts at  $I = 1$  mA, which corresponds to  $H^{\text{Oe}} \approx 0.04$  mT (0.015 mT) averaged over the sample area for sample A (B). These estimates are reasonably consistent with the measured values of 0.07 mT (0.03 mT). Finally, we determine  $H^{\text{so}}$  as an average of  $H^{\text{eff}}$  between the two current directions. The spin-orbit field depends linearly on  $j$ , as expected for strain-related spin-orbit interactions:  $dH^{\text{so}}/dj = 0.53 \times 10^{-9}$  and  $0.23 \times 10^{-9} \text{ T cm}^2 \text{ A}^{-1}$  for samples A and B respectively.

We now compare the experimentally measured  $H^{\text{so}}$  with theoretically calculated effective spin-orbit field. In (Ga,Mn)As, the only term allowed by symmetry that generates  $H^{\text{so}}$  linear in the electric current is the  $\Omega_e$  term, which results in the directional dependence of  $\mathbf{H}^{\text{so}}$  on  $\mathbf{j}$  precisely as observed in

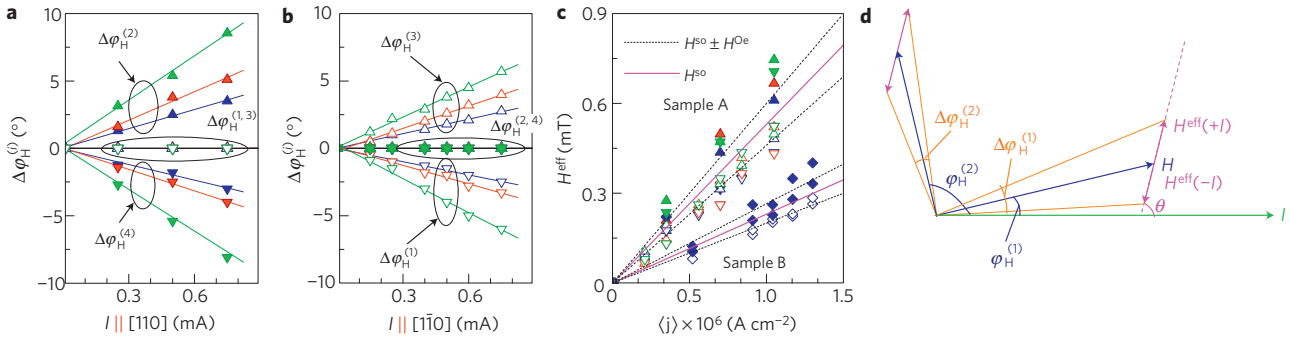


**Figure 3 | Determination of current-induced effective spin-orbit magnetic field.** **a, b**, Difference in switching angles for opposite current directions  $\Delta\varphi_H^{(j)}$  as a function of  $I$  for sample A for different external fields  $H$  for orthogonal current directions. **c**, The measured effective field  $H^{\text{eff}} = H^{\text{so}} \pm H^{\text{Oe}}$  as a function of average current density  $\langle j \rangle$  for sample A (triangles) and sample B (diamonds). **d**, Schematic diagram of the different angles involved in determining  $H^{\text{eff}}$ :  $\varphi_H$  is the angle between current  $\mathbf{I}$  and external magnetic field  $\mathbf{H}$ ;  $\Delta\varphi_H$  is the angle between total fields  $\mathbf{H} + \mathbf{H}^{\text{eff}}(+I)$  and  $\mathbf{H} + \mathbf{H}^{\text{eff}}(-I)$  and  $\theta$  is the angle between  $\mathbf{I}$  and  $\mathbf{H}^{\text{eff}}(+I)$ .

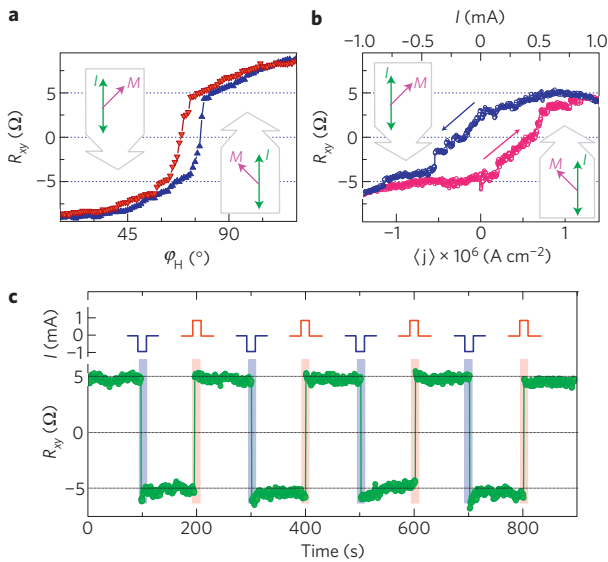


**Figure 4 | Current-induced reversible magnetization switching.** **a**,  $\varphi_H$  dependence of  $R_{xy}$  near the  $[010] \rightarrow [\bar{1}00]$  magnetization switching for  $I = \pm 0.7$  mA in sample A for  $\mathbf{I} \parallel [\bar{1}10]$ . **b**,  $R_{xy}$  shows hysteresis as a function of current for a fixed field  $H = 6$  mT applied at  $\varphi_H = 72^\circ$ . **c**, Magnetization switches between the  $[010]$  and  $[\bar{1}00]$  directions when alternating  $\pm 1.0$  mA current pulses are applied. The pulses have 100 ms duration and are shown schematically above the data curve.  $R_{xy}$  is measured with  $I = 10 \mu\text{A}$ .

experiment. As for the magnitude of  $H^{\text{so}}$ , for three-dimensional  $J = 3/2$  holes we obtain

$$\mathbf{H}^{\text{so}}(\mathbf{E}) = \frac{eC\Delta\varepsilon}{g^*\mu_B} \frac{(-38n_h\tau_h + 18n_l\tau_l)}{217(n_h + n_l)} \cdot (E_x, -E_y, 0)$$

where  $\mathbf{E}$  is the electric field,  $g^*$  is the Luttinger Landé factor for holes,  $\mu_B$  is the Bohr magneton and  $n_{h,l}$  and  $\tau_{h,l}$  are densities and lifetimes for the heavy (h) and light (l) holes. Detailed derivation of  $H^{\text{so}}$  is given in the Supplementary Information. Using this result, we estimate  $dH^{\text{so}}/dj = 0.6 \times 10^{-9}$  T  $\text{cm}^2 \text{A}^{-1}$  assuming  $n_h = n \gg n_l$  and  $\tau_h = m_h/(e^2\rho n)$ , where  $\rho$  is the resistivity measured experimentally, and using  $\Delta\varepsilon = 10^{-3}$ ,  $n = 2 \times 10^{20} \text{ cm}^{-3}$ . The agreement between theory and experiment is excellent. It is important to note, however, that we used GaAs band parameters<sup>25</sup>  $m_h = 0.4 m_0$ , where  $m_0$  is the free electron mass,  $g^* = 1.2$  and  $C = 2.1 \text{ eV \AA}$ . Although the corresponding parameters for (Ga,Mn)As are not known, the use of GaAs parameters seems reasonable. We note, for example,

that GaAs parameters adequately described tunnelling anisotropic magnetoresistance in recent experiments<sup>26</sup>.

Finally, we demonstrate that the current-induced effective spin-orbit field  $H^{\text{so}}$  is sufficient to reversibly manipulate the direction of magnetization. Figure 4a shows the  $\varphi_H$  dependence of  $R_{xy}$  for sample A, showing the  $[010] \rightarrow [\bar{1}00]$  magnetization switching. If we fix  $H = 6$  mT at  $\varphi_H = 72^\circ$ ,  $R_{xy}$  forms a hysteresis loop as current is swept between  $\pm 1$  mA.  $R_{xy}$  is changing between  $\pm 5 \Omega$ , indicating that  $\mathbf{M}$  is switching between the  $[010]$  and  $[\bar{1}00]$  directions. Short (100 ms) 1 mA current pulses of alternating polarity are sufficient to permanently rotate the direction of magnetization. The device thus performs as a non-volatile memory cell, with two states encoded in the magnetization direction, the direction being controlled by the unpolarized current passing through the device. The device can be potentially operated as a four-state memory cell if both the  $[110]$  and  $[\bar{1}10]$  directions can be used to inject current. We find that we can reversibly switch the magnetization with currents as low as 0.5 mA (current densities  $7 \times 10^5 \text{ A cm}^{-2}$ ), an order of magnitude smaller than by polarized current injection in ferromagnetic metals<sup>1–3</sup>, and just a few times larger than by externally polarized current injection in ferromagnetic semiconductors<sup>4</sup>.

## Methods

The (Ga,Mn)As wafers were grown by molecular beam epitaxy at 265 °C and subsequently annealed at 280 °C for 1 h in nitrogen atmosphere. Sample A was fabricated from a 15-nm-thick epilayer with 6% Mn, and sample B from a 10-nm-thick epilayer with 7% Mn. Both wafers have a Curie temperature  $T_c \approx 80$  K. The devices were patterned into 6- and 10- $\mu\text{m}$ -diameter circular islands to decrease domain pinning. Cr/Zn/Au (5 nm/10 nm/300 nm) ohmic contacts were thermally evaporated. All measurements were carried out in a variable-temperature cryostat at  $T = 40$  K for sample A and at 25 K for sample B, well below the temperature of (Ga,Mn)As-specific cubic-to-uniaxial magnetic anisotropy transitions<sup>27</sup>, which has been measured to be 60 and 50 K for the two wafers. The temperature rise for the largest currents used in the reported experiments was measured to be  $< 3$  K.

Transverse anisotropic magnetoresistance  $R_{xy} = V_y/I_x$  is measured using the four-probe technique, which ensures that possible interfacial resistances, for example, those related to the antiferromagnetic ordering in the Cr wetting layer<sup>28</sup>, do not contribute to the measured  $R_{xy}$ . The d.c. current  $I_x$  was applied either along the  $[110]$  (contacts 4–8 in Fig. 1a) or along the  $[1\bar{1}0]$  (contacts 2–6) direction. Transverse voltage was measured in the Hall configuration, for example, between contacts 2–6 for  $I_x \parallel [110]$ . To ensure uniform magnetization of the island, magnetic field was ramped to 0.5 T after adjusting the current at the beginning of each field rotation scan. We monitor  $V_x$  between different contact sets (for example, 1–7, 4–6 and 3–5) to confirm the uniformity of magnetization within the island.

To determine the direction of magnetization  $\mathbf{M}$ , we use the dependence of  $R_{xy}$  on magnetization<sup>29</sup>:

$$R_{xy} = \Delta\rho \sin\varphi_M \cos\varphi_M$$

where  $\Delta\rho = \rho_{\parallel} - \rho_{\perp}$ ,  $\rho_{\parallel} < \rho_{\perp}$  are the resistivities for magnetization oriented parallel and perpendicular to the current, and  $\varphi_M = \angle \mathbf{M} \mathbf{I}$  is an angle between magnetization and current. In a circular sample, the current distribution is

non-uniform and the angle between the magnetization and the local current density varies throughout the sample. However, the resulting transverse anisotropic magnetoresistance depends only on  $\varphi_M$ . For the current-to-current-density conversion, we model our sample as a perfect disc with two point contacts across the diameter. The average current density in the direction of current injection is  $\langle j \rangle = 2I/(\pi ad)$ , where  $a$  is the disc radius and  $d$  is the (Ga,Mn)As layer thickness. In a real sample, the length of contact overlap with (Ga,Mn)As ensures that  $j$  changes by less than a factor of 3 throughout the sample. A detailed discussion of the current distribution and of measurements of joule heating can be found in the Supplementary Information.

Received 17 December 2008; accepted 2 July 2009;  
published online 2 August 2009

## References

- Slonczewski, J. C. Current-driven excitation of magnetic multilayers. *J. Magn. Magn. Mater.* **159**, 1–7 (1996).
- Berger, L. Emission of spin waves by a magnetic multilayer traversed by a current. *Phys. Rev. B* **54**, 9353–9358 (1996).
- Myers, E. B., Ralph, D. C., Katine, J. A., Louie, R. N. & Buhrman, R. A. Current-induced switching of domains in magnetic multilayer devices. *Science* **285**, 867–870 (1999).
- Chiba, D., Sato, Y., Kita, T., Matsukura, F. & Ohno, H. Current-driven magnetization reversal in a ferromagnetic semiconductor (Ga,Mn)As/GaAs/(Ga,Mn)As tunnel junction. *Phys. Rev. Lett.* **93**, 216602 (2004).
- Aronov, A. G. & Lyanda-Geller, Y. B. Nuclear electric resonance and orientation of carrier spins by an electric field. *JETP Lett.* **50**, 431–434 (1989).
- Edelstein, V. M. Spin polarization of conduction electrons induced by electric current in two-dimensional asymmetric electron systems. *Solid State Commun.* **73**, 233–235 (1990).
- Kalevich, V. K. & Korenev, V. L. Effect of electric field on the optical orientation of 2d electrons. *JETP Lett.* **52**, 230–235 (1990).
- Kato, Y., Myers, R. C., Gossard, A. C. & Awschalom, D. D. Coherent spin manipulation without magnetic fields in strained semiconductors. *Nature* **427**, 50–53 (2004).
- Silov, A. Y. *et al.* Current-induced spin polarization at a single heterojunction. *Appl. Phys. Lett.* **85**, 5929–5931 (2004).
- Ganichev, S. D. Spin-galvanic effect and spin orientation by current in non-magnetic semiconductors. *Int. J. Mod. Phys. B* **22**, 1–26 (2008).
- Meier, L. *et al.* Measurement of Rashba and Dresselhaus spin-orbit magnetic fields. *Nature Phys.* **3**, 650–654 (2007).
- Dresselhaus, G. Spin-orbit coupling effects in zinc blende structures. *Phys. Rev.* **100**, 580–586 (1955).
- Bir, G. L. & Pikus, G. E. *Symmetry and Strain-Induced Effects in Semiconductors* (Wiley, 1974).
- Bychkov, Y. A. & Rashba, E. I. Oscillatory effects and the magnetic susceptibility of carriers in inversion layers. *J. Phys. C: Solid State Phys.* **17**, 6039–6045 (1984).
- Aronov, A. G., Lyanda-Geller, Y. B. & Pikus, G. E. Spin polarization of electrons by an electric current. *Sov. Phys. JETP* **73**, 537–541 (1991).
- Golub, L. E. *et al.* Electric current-induced spin orientation in quantum well structures. *J. Magn. Magn. Mater.* **300**, 127–131 (2006).
- Wilamowski, Z., Malissa, H., Schaffler, F. & Jantsch, W. g-factor tuning and manipulation of spins by an electric current. *Phys. Rev. Lett.* **98**, 187203 (2007).
- Ohno, H. *et al.* (Ga,Mn)As: A new diluted magnetic semiconductor based on GaAs. *Appl. Phys. Lett.* **69**, 363–365 (1996).
- Ohno, H. Making nonmagnetic semiconductors ferromagnetic. *Science* **281**, 951–956 (1998).
- Dietl, T., Ohno, H., Matsukura, F., Cibert, J. & Ferrand, D. Zener model description of ferromagnetism in zinc-blende magnetic semiconductors. *Science* **287**, 1019–1022 (2000).
- Berciu, M. & Bhatt, R. N. Effects of disorder on ferromagnetism in diluted magnetic semiconductors. *Phys. Rev. Lett.* **87**, 107203 (2001).
- Welp, U., Vlasko-Vlasov, V. K., Liu, X., Furdyna, J. K. & Wojtowicz, T. Magnetic domain structure and magnetic anisotropy in  $\text{Ga}_{1-x}\text{Mn}_x\text{As}$ . *Phys. Rev. Lett.* **90**, 167206 (2003).
- Liu, X., Sasaki, Y. & Furdyna, J. K. Ferromagnetic resonance in  $\text{Ga}_{1-x}\text{Mn}_x\text{As}$ : Effects of magnetic anisotropy. *Phys. Rev. B* **67**, 205204 (2003).
- Overby, M., Chernyshov, A., Rokhinson, L. P., Liu, X. & Furdyna, J. K. GaMnAs-based hybrid multiferroic memory device. *Appl. Phys. Lett.* **92**, 192501 (2008).
- Chantis, A. N. *et al.* Strain-induced conduction-band spin splitting in GaAs from first-principles calculations. *Phys. Rev. B* **78**, 075208 (2008).
- Elsen, M. *et al.* Exchange-mediated anisotropy of (Ga,Mn)As valence-band probed by resonant tunneling spectroscopy. *Phys. Rev. Lett.* **99**, 127203 (2007).
- Chiba, D. *et al.* Magnetization vector manipulation by electric fields. *Nature* **455**, 515–518 (2008).
- Smit, P. & Alberts, H. L. On magnetic transitions in dilute Cr–Ga and Cr–Ge alloys. *J. Appl. Phys.* **63**, 3609–3610 (1988).
- Tang, H. X., Kawakami, R. K., Awschalom, D. D. & Roukes, M. L. Giant planar Hall effect in epitaxial (Ga,Mn)As devices. *Phys. Rev. Lett.* **90**, 107201 (2003).

## Acknowledgements

This work was supported in part by NSF under the grants ECS-0348289 (L.P.R.) and DMR-0603752 (J.K.F.).

## Author contributions

A.C. and M.O. fabricated samples and carried out measurements, X.L. and J.K.F. designed and grew (Ga,Mn)As wafers specifically for these experiments, Y.L.-G. developed the theory and L.P.R. designed and supervised the experiments.

## Additional information

Supplementary information accompanies this paper on [www.nature.com/naturephysics](http://www.nature.com/naturephysics). Reprints and permissions information is available online at <http://npg.nature.com/reprintsandpermissions>. Correspondence and requests for materials should be addressed to L.P.R.